

Article

Enhancement of Electromagnetic Wave Shielding Effectiveness by the Incorporation of Carbon Nanofibers–Carbon Microcoils Hybrid into Commercial Carbon Paste for Heating Films

Gi-Hwan Kang¹, Sung-Hoon Kim^{1,*} , Ji-Hun Kang¹, Junwoo Lim¹, Myeong Ho Yoo² and Yi Tae Kim²¹ Department of Energy and Chemical Engineering, Silla University, Busan 46958, Republic of Korea² Department of Research and Development, SH Korea Co. Ltd., Busan 49500, Republic of Korea

* Correspondence: shkim@silla.ac.kr; Tel.: +82-51-999-5619

Abstract: Carbon microcoils (CMCs) were formed on stainless steel substrates using $C_2H_2 + SF_6$ gas flows in a thermal chemical vapor deposition (CVD) system. The manipulation of the SF_6 gas flow rate and the SF_6 gas flow injection time was carried out to obtain controllable CMC geometries. The change in CMC geometry, especially CMC diameter as a function of SF_6 gas flow injection time, was remarkable. In addition, the incorporation of H_2 gas into the $C_2H_2 + SF_6$ gas flow system with cyclic SF_6 gas flow caused the formation of the hybrid of carbon nanofibers–carbon microcoils (CNFs–CMCs). The hybrid of CNFs–CMCs was composed of numerous small-sized CNFs, which formed on the CMCs surfaces. The electromagnetic wave shielding effectiveness (SE) of the heating film, made by the hybrids of CNFs–CMCs incorporated carbon paste film, was investigated across operating frequencies in the 1.5–40 GHz range. It was compared to heating films made from commercial carbon paste or the controllable CMCs incorporated carbon paste. Although the electrical conductivity of the native commercial carbon paste was lowered by both the incorporation of the CMCs and the hybrids of CNFs–CMCs, the total SE values of the manufactured heating film increased following the incorporation of these materials. Considering the thickness of the heating film, the presently measured values rank highly among the previously reported total SE values. This dramatic improvement in the total SE values was mainly ascribed to the intrinsic characteristics of CMC and/or the hybrid of CNFs–CMCs contributing to the absorption shielding route of electromagnetic waves.

Keywords: controllable carbon microcoils; hybrid of carbon nanofibers–carbon microcoils; carbon paste; heating film; electromagnetic wave; shielding effectiveness; absorption shielding route



Citation: Kang, G.-H.; Kim, S.-H.; Kang, J.-H.; Lim, J.; Yoo, M.H.; Kim, Y.T. Enhancement of Electromagnetic Wave Shielding Effectiveness by the Incorporation of Carbon Nanofibers–Carbon Microcoils Hybrid into Commercial Carbon Paste for Heating Films. *Molecules* **2023**, *28*, 870. <https://doi.org/10.3390/molecules28020870>

Academic Editor: Elena Cariati

Received: 17 December 2022

Revised: 8 January 2023

Accepted: 11 January 2023

Published: 15 January 2023



Copyright: © 2023 by the authors. Licensee MDPI, Basel, Switzerland. This article is an open access article distributed under the terms and conditions of the Creative Commons Attribution (CC BY) license (<https://creativecommons.org/licenses/by/4.0/>).

1. Introduction

The trend toward miniaturization and multifunctionality of electronic devices has exacerbated the problem of electromagnetic interference (EMI). As the applicable frequency range of electronic devices enters the higher frequency region, the shielding of electromagnetic wave radiation emitted from electronic devices is required to prevent not only the malfunction of other electronics, but also a significant threat to human health. This is because increased exposure can cause the device to malfunction and affect human health. The only solution to prevent damage from harmful radiation and protect electronics is to provide a shield that filters out the interference.

The shielding of electromagnetic waves typically proceeds via three main routes: reflection loss, absorption loss, and internal reflection loss [1]. For an absorption loss route greater than 10 dB, reflection and absorption loss routes are usually regarded as the main shielding routes [1–4]. In the relatively low-frequency range (typically less than 2.0 GHz), the reflection loss route is thought to be the crucial mechanism for preventing EMI [4,5]. However, at high operating frequencies (above 2.0 GHz), the absorption loss route is considered the main mechanism for preventing EMI [4,5]. High electrical conductivity is the key parameter for the shielding mechanism via the reflection loss route, while both high

electrical conductivity and high magnetic permeability are important parameters for the shielding mechanism through the absorption loss route [1,5]. Therefore, in a relatively low frequency range, conductive metals, such as copper and aluminum, seem to be appropriate materials for EMI shielding via the reflection loss route. However, at higher operating frequencies, carbon-based materials would be the optimal materials through the absorption loss route because carbon-based materials can possess high magnetic field characteristics. Furthermore, carbon-based materials are lightweight and moldable [6–8]. Therefore, carbon-based materials are preferred as optimal materials for electromagnetic wave shielding in the relatively high operating frequency range for portable electronics, automobile electronics, and avionic electronic devices [5,9–11].

Recently, carbon-based heating films have been introduced as replacements for conventional heating systems [12–17]. They commonly consist of a substrate film made from polymers such as polyethylene terephthalate (PET). Next, they are coated with electrically resistive materials and are electrically contacted by busbars. The applicable materials for carbon-based heating films include carbon nanotubes (CNTs) [12,13], graphene oxide [14], reduced graphene oxide [15,16], and graphene nanoplatelets (GNPs) [17]. The materials used in busbars are commonly composed of silver, aluminum, and copper, and are laminated with another layer of insulating film, usually having similar characteristics to the substrate. Conductive polymers can occasionally be used together with carbon-based nanomaterials to improve the electrical conductivity of carbon-based films [18]. Thus, carbon-based heating films are made of stacks comprised of many individual functional films, which can give rise to efficient heat-dissipating capabilities. This heating film system has several advantages, such as energy savings, eco-friendliness, and durability. A difficult problem in the application of a heating film is the shielding of electromagnetic waves emitted from the heating source in the film.

To date, there are some reports of heating films being used to shield against electromagnetic interference. Lee et al. registered a patent concerning a film-type planar heating element that can be used to prevent electromagnetic waves from generating heat in the form of multiple layers of films [19]. Kim et al., registered a patent for a production method of heating films to be used in electromagnetic wave shielding applications [20]. Kang et al. suggested a method for generating heat on a large-area graphene film more efficiently by utilizing the unique electromagnetic wave absorption properties of graphene [21].

Lin et al. showed that graphene exhibits a higher electron shielding effect than CNT. In addition, it was shown that when CNT and graphene were hybridized, electrical conductivity was improved by about eight times [22]. In previous research results, materials with a three-dimensional structure, compared to one-dimensional shielding materials, have higher electromagnetic wave shielding effects [23]. We introduce carbon microcoils (CMCs)-related materials, as a three-dimensional structure, in the manufacturing of heating films which can be used as shielding agents against electromagnetic waves. CMCs exhibit unique helical geometries [24]. When an incoming electromagnetic wave reaches the CMCs, electric current flows through helically oriented individual carbon fibers (CFs) situated on the CMCs, thereby inducing an electromotive force and generating a variable magnetic field [25–27]. Finally, the incoming electromagnetic wave energy is absorbed into the unique geometries of CMCs and converted into thermal energy [26]. Previously, we reported an increase in the shielding effectiveness (SE) of the CMCs–polyurethane composites with increasing content of CMCs [28]. Kim et al. reported that the SE of a hybridized carbon microcoil–carbon fiber nonwoven fabric increased slightly [29]. In addition, diverse hybrid formations using carbon-based materials have been developed to enhance the SE values [29–31]. These combined results clearly suggest that the formation of CMCs-related materials could enhance SE values.

In the present work, controllable CMCs were obtained by manipulating the additive gas, SF₆, and flow injection time. In addition, the hybrid formation of numerous small carbon nanofibers (CNFs) on the surfaces of CMCs (CNFs–CMCs) can be achieved by the injection of H₂ flow with the cyclic process of SF₆ flow. The SE of the heating film made

from the CNFs–CMCs hybrid material incorporated with carbon paste was investigated across the operating frequencies in the 1.5–40 GHz range. The results were compared with those for heating films made using a native commercial carbon paste or controllable CMCs-incorporated carbon paste. The morphologies and electrical conductivities of different types of heating films were investigated. The main shielding mechanism of the heating film made from the hybrids of CNFs–CMCs incorporated carbon paste is suggested and discussed.

2. Results and Discussion

Figure 1 shows the magnified FESEM images of the surface morphologies for samples A–I. Under a flow rate of 20 sccm SF_6 , the diameters of the CMCs increased with the SF_6 flow injection time (see Figure 1a–c). Under the 50 sccm and 100 sccm SF_6 flow rates, the CMCs diameters also tended to increase with increasing SF_6 flow injection time (see Figure 1d–f and Figure 1g–i, respectively). This reveals that the lowest SF_6 flow injection time in this study (5 min) can give rise to the CMCs with the smallest diameters, irrespective of the SF_6 flow rate. In addition, Figure 1 shows that overall the diameters of the CMCs are independent of the SF_6 flow rate. These results strongly suggest that the SF_6 flow injection time, instead of the SF_6 flow rate, can directly influence the formation of CMCs with a specific diameter.

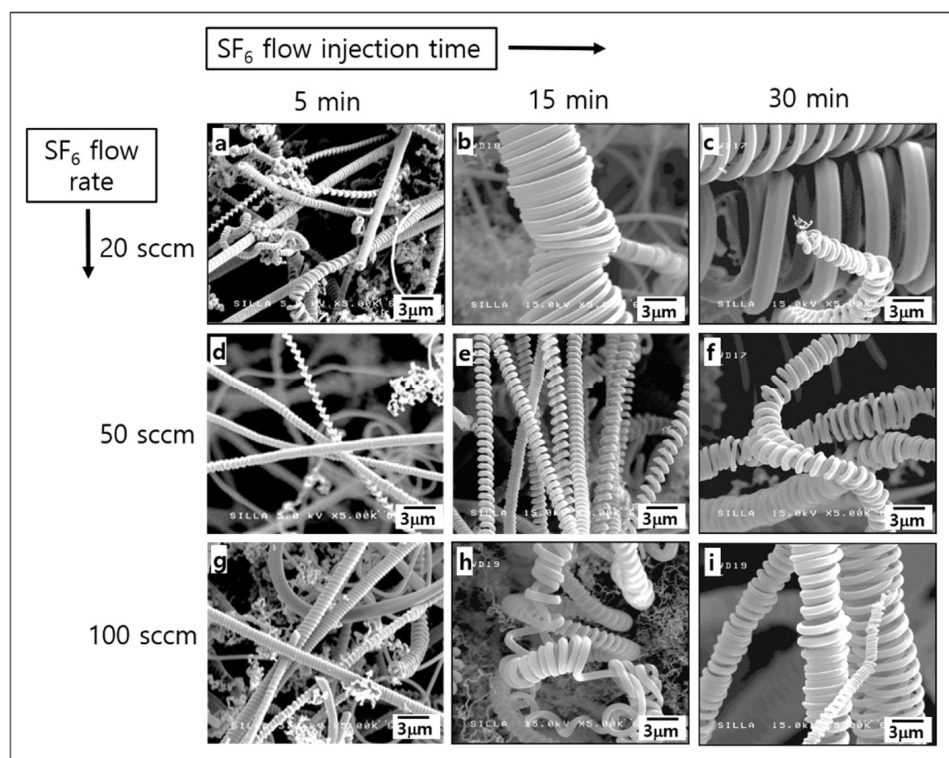


Figure 1. The FESEM images of the surface morphologies for samples (a) A, (b) B, (c) C, (d) D, (e) E, (f) F, (g) G, (h) H, and (i) I.

Figure 2 shows FESEM images of sample J, which were obtained by the injection of H_2 flow and the cyclic process of SF_6 flow. As shown in Figure 2a, a woolen yarn-type surface is present in sample J. The magnified FESEM image of sample J also indicated the existence of many small-sized CNFs on the CMCs surfaces (see Figure 2b,c). As previously reported, the small-sized CNFs around the CMCs seem to have a hybridized aspect between the CNFs and CMCs by the cyclic process of SF_6 flow [32–40]. This result suggests that the cyclic SF_6 flow with the injection of H_2 gas could produce CNFs–CMCs hybrids [40].

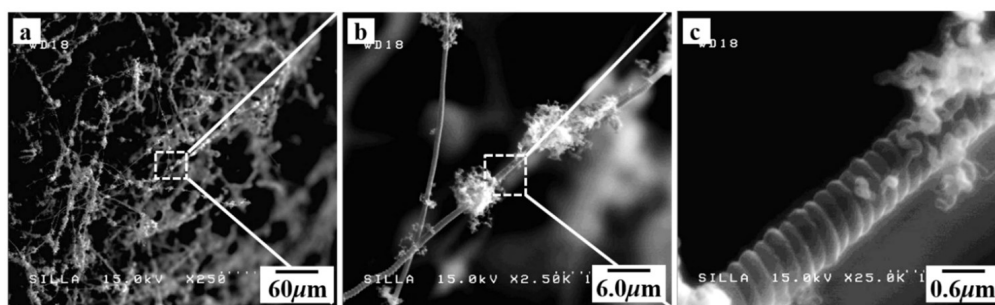


Figure 2. (a) The FESEM image of the surface morphology for sample J, (b) the magnified-FESEM image of the squared-area in (a), and (c) the high magnified-FESEM image of the squared-area in (b).

The presence of different nanocarbon formation attributes in sample J compared to samples A–I can be explained as follows. It is known that producing a hybrid nanocarbon from typical nanocarbon materials, such as CNTs with CNFs and CMCs with carbon nanocoils, is very difficult because the transition metals used as catalysts to promote hybrid nanocarbon growth tend to easily diffuse into the interior of the carbon substrate during the reaction [41,42]. For the surfaces of CMCs during the reaction, the tiny Ni catalysts used for hybrid nanocarbon growth would not be sufficient because tiny Ni catalysts could easily diffuse into the interior of CMCs in an amorphous solid state [43–45]. Consequently, numerous small-sized CNFs could not be formed on the surfaces of the CMCs of samples A–I because of the lack of tiny Ni catalysts on the surfaces of the CMCs during the reaction.

However, a previous report revealed that the injection of H_2 gas into the flow of C_2H_2 , and an abundant C_2H_2 gas flow relative to the SF_6 gas flow in the reaction environment are known to facilitate the formation of numerous small-sized CNFs by the generation of numerous tiny Ni catalysts from large-sized Ni catalysts [46]. In this work, the H_2 flow injection for sample J was subjected to the injection of H_2 flow into the C_2H_2 flow. Furthermore, the cyclic process in sample J could produce an abundant C_2H_2 flow environment compared with SF_6 gas flow, especially during the SF_6 flow-off period [40]. Compared to samples A–I, sample J produced a much higher number of tiny Ni catalysts, which could readily be placed on the surfaces of the CMCs. Consequently, this would result in the formation of small-sized CNFs on the surfaces of the CMCs owing to the increased number of tiny Ni catalysts, probably enough to overcome the insufficiency of Ni catalysts on the surfaces of the CMCs. This can be attributed to the diffusion of Ni catalysts into the interior of the CMCs during the reaction.

Figure 3 shows systematic diagrams for the formation of samples A–I ($C_2H_2 + SF_6$ gas flow system without cyclic process of SF_6 gas flow, Figure 3a) and sample J ($C_2H_2 + SF_6 + H_2$ gas flow system with a cyclic process of SF_6 gas flow, Figure 3b). Ni fragments were located merely on the heads of CMCs for samples A–I (Figure 3a). However, for Sample J, Ni fragments were present on the CMC head and the tiny-sized Ni fragments were present on the CMC surface. Moreover, the numerous tiny Ni fragments, produced by the injection of H_2 gas into the C_2H_2 flow during the cyclic addition of SF_6 , were present on the surfaces of the CMCs as shown in Figure 3b.

For the mass production of CMCs-related nanocarbon samples, we chose the conditions of samples E and J among the various types of CMCs-related nanocarbon formation reaction conditions. Almost 19 g of CMCs per approximately 0.6 g Ni catalyst could be obtained in a one-batch reaction, as shown in Figure 4a. Figure 4b–d show the FESEM images of these CMCs samples. The obtained sample seemed to have CMCs with fixed diameters within the range of 1–5 μm . The magnified FESEM image of this sample (Figure 4d) clearly indicated the formation of well-developed controllable CMCs geometries under these reaction conditions.

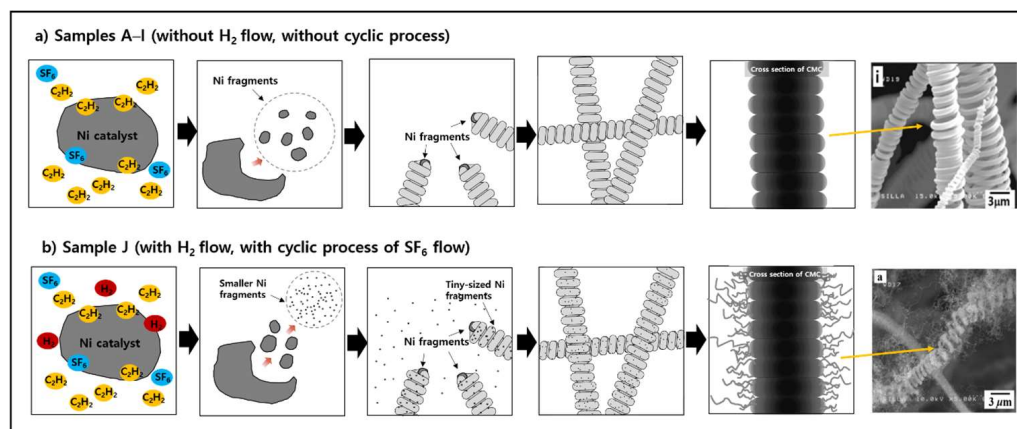


Figure 3. Systematic diagrams indicating (a) the formation of controllable CMCs in the C₂H₂ + SF₆ gas flow system and (b) the formation of numerous small-sized CNFs on the surfaces of CMCs caused by H₂ flow injection and the abundant C₂H₂ flow during SF₆ flow off period in the cyclic process.

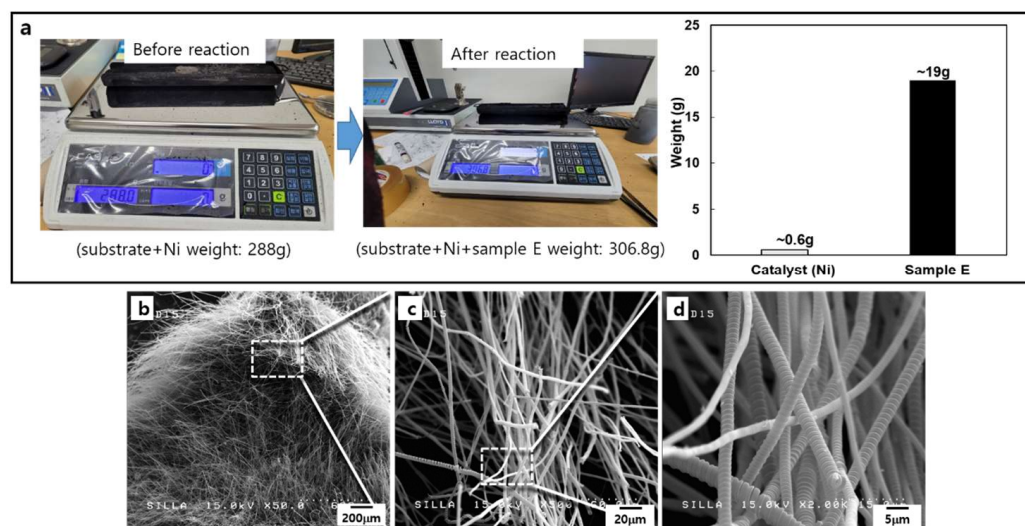


Figure 4. (a) Optical photograph for the weighting of sample E, (b) FESEM image of sample E, (c) magnified-FESEM image of (b), and (d) high magnified-FESEM image of (c).

Under the experimental conditions of sample J, approximately 20 g of the hybrids of CNFs–CMCs per approximately 0.6 g Ni catalyst could be obtained in a one-batch reaction, as shown in Figure 5a. Figure 5b–d clearly show the formation of hybridized CNFs–CMCs between the numerous small-sized CNFs and CMCs.

After achieving mass production of CMCs-related materials, we made a blend of 30 wt% sample J with 70 wt% commercial carbon paste. A blend of 30 wt% sample E with 70 wt% commercial carbon paste was also prepared to compare the SE values of samples J and E. These blends were coated on a PET film by a commonly used printing method using a spatula blade. Figure 6 shows the SE values of these coated PET films across the operating frequencies in the 1.5–40 GHz range.

Compared with the total SE values of the PET film coated with 30 wt% sample E-incorporated carbon paste (see Table 1), the value of the PET film coated with 30 wt% sample J-incorporated carbon paste was more than two-fold higher in dB scale across the entire operating frequency range, as shown in Figure 6.

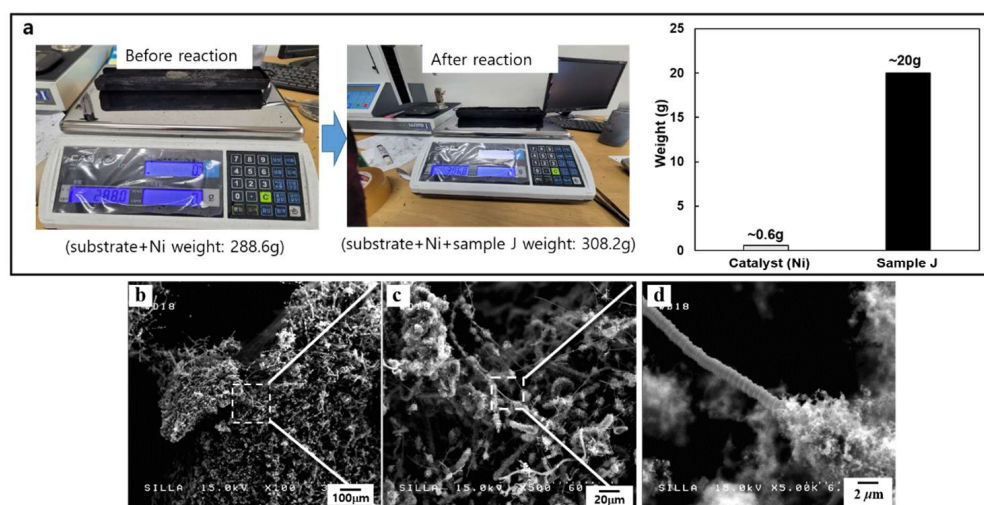


Figure 5. (a) Optical photograph for the weighting of sample J, (b) FESEM image of sample E, (c) magnified-FESEM image of (b), and (d) high magnified-FESEM image of (c).

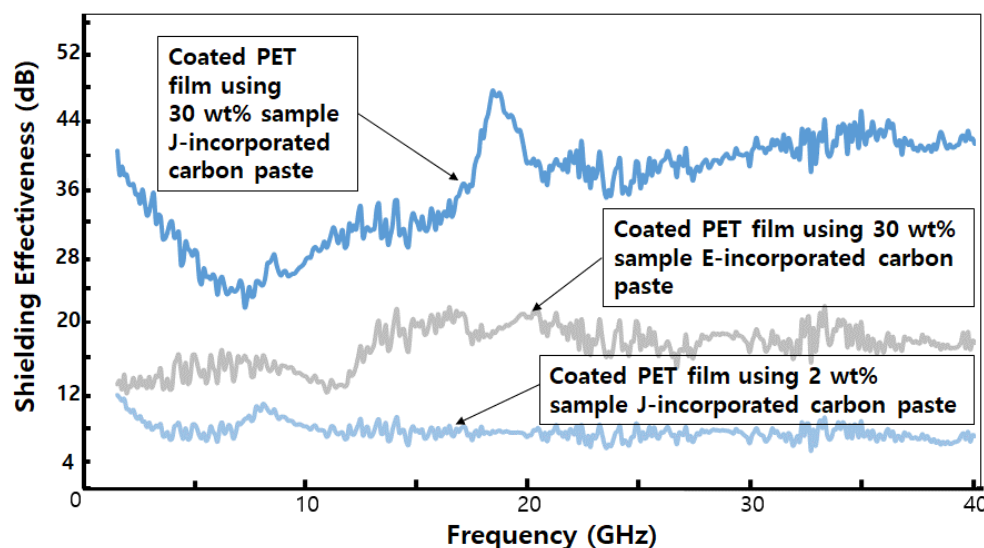


Figure 6. The total SE values of the coated PET films using the blends of CMCs-related materials and commercial carbon pastes.

Table 1. Thickness, electrical resistivity, and electrical conductivity of the coated PET films by commercial carbon paste, 30 wt% sample E-incorporated carbon paste, and 30 wt% sample J-incorporated carbon paste.

The Coated PET Films and Type of Carbon Paste	Thickness t (mm)	Electrical Resistivity ρ ($\Omega \cdot m$)	Electrical Conductivity σ (S/m)	Correction Factor * F (F/w)
Commercial carbon paste	0.6 (± 0.04)	$2.42 (\pm 0.15) \times 10^{-4}$	$4.13 (\pm 0.08) \times 10^3$	0.98
30 wt% sample E-incorporated carbon paste	0.6 (± 0.07)	$5.43 (\pm 1.22) \times 10^{-4}$	$1.84 (\pm 0.46) \times 10^3$	0.79
30 wt% sample J-incorporated carbon paste	0.6 (± 0.05)	$4.61 (\pm 0.65) \times 10^{-4}$	$2.17 (\pm 0.23) \times 10^3$	0.79

* Correction factor was calculated from Table 2 in Ref. [32].

Table 2. EMI SE of carbon-based materials.

Carbon-Based Materials	Thickness (mm)	Electrical Conductivity or Resistivity	Operating Frequency (GHz)	SE (dB)	SE/Thickness (dB/mm)	Ref.
CNT/*MCMB	0.15–0.6	1100 S/m		31–56	93–206	[47]
15 wt% *CNF/*ABS		$1.5 \pm 0.1 \Omega \cdot \text{cm}$		35	31.8	
15 wt% CNT/*ABS	1.1	$0.81 \pm 0.05 \Omega \cdot \text{cm}$	8.2–12.4	51	46.4	[48]
*CNF/epoxy	2.1	-		5–34	2.4–16.2	[49]
GNP/*PEDOT:PSS	0.8	684 S/m		70	88	[50]
*SCF/*EVA	3.5	-		29.5–34.1	8.4–9.7	[51]
*MX/*RGO	3	1000 S/m	8–12	51	17	[52]
*3D G–CNT–Fe ₂ O ₃	0.6	22,781 S/m		130–134	216–223	[53]
*GN/Cu	0.009 (± 0.0015)	$5.88 (\pm 0.29) \times 10^6 \text{ S/m}$	1–18	52–63	5777–7000	[54]
*SWCNT/epoxy	1.5	20 S/m	0.01–1.5	15–49	10–32.6	[55]
The coated PET film using 30 wt% sample E-incorporated carbon paste	0.6	1840 S/m		12–24	20–40	
The coated PET film using 30 wt% sample J-incorporated carbon paste	0.6	2170 S/m	1.5–40	24–56	40.0–93.3	This work

*CNT: carbon nanotube, *MCMB: mesocarbon microbeads, *CB: carbon black, *CNF: carbon nanofiber, *ABS: acrylonitrile–butadiene–styrene, *PEDOT:PSS: poly(3,4-ethylenedioxythiophene)–poly(styrene-sulfonate), *SCF: short carbon fiber, *EVA: ethylene vinyl acetate, *MX: Mxene, *RGO: reduced graphene oxide, *3D G–CNT–Fe₂O₃: three-dimensional graphene–carbon nanotube–iron oxide, *GN: graphene, *SWCNT: single wall carbon nanotube.

This dramatic increase in the total SE values of the coated PET film by 30 wt% sample J-incorporated carbon paste seems to be partly ascribed to the enhanced electrical conductivity (from $(1.84 \pm 0.46) \times 10^3 \text{ S/m}$ to $(2.17 \pm 0.23) \times 10^3 \text{ S/m}$, see Table 2) by the hybrid formation between the numerous small-sized CNFs and the CMCs in sample J, as in a previous report [30]. Furthermore, the numerous small-sized CNFs on the surfaces of the CMCs in sample J intersected with one another. When an incoming electromagnetic wave reaches these intersected-CNFs, electric current flows into the intersections and dissipates in various directions, thereby inducing an electromotive force and generating a variable magnetic field [25]. The geometry of these CNFs holds and rotates incoming electromagnetic waves within the generated variable magnetic field. Thus, the incoming electromagnetic wave energy is absorbed into these CNFs and is finally converted into thermal energy [26]. Therefore, these intersections can contribute to the absorption mechanism for shielding against electromagnetic waves. Consequently, the total SE values of the PET film coated with the 30 wt% sample J-incorporated carbon paste were higher than those of the 30 wt% sample E-incorporated carbon paste. This matches the measured SE values shown in Figure 6. The skin depth (δ) of a shielding material is defined as $\delta = (\pi f \mu)^{-1/2}$ [2], indicating that δ^2 is inversely proportional to the electrical conductivity (σ), frequency (f), and magnetic permeability (μ). Therefore, higher magnetic permeability can efficiently reduce the skin depth of the shielding material, thereby enhancing the SE values. The intrinsic characteristics of CMCs, and the aspect of numerous small-sized CNFs intersecting with one another in sample J, can enhance the magnetic field and then absorb incoming EM waves. Consequently, they can enhance magnetic permeability (μ), resulting in an improvement in the absorption loss of electromagnetic waves. Therefore, the SE values of the PET film coated with the 30 wt% sample J-incorporated carbon paste were

much higher than those of the 30 wt% sample E-incorporated carbon paste across the entire operating frequency range.

Indeed, the PET film coated with 30 wt% sample J-incorporated carbon paste had total SE values above 20 dB throughout the entire range of operating frequencies. Compared with the previously reported total SE values, the presently measured values seem to be ranked in the top tier (see Table 2). Therefore, we suggest that the hybridized CNFs–CMCs sample can be effectively used in diverse industrial fields.

A blend of 2 wt% sample J with 98 wt% commercial carbon paste was also prepared to determine the optimal amount of sample J to add to the commercial carbon paste. Indeed, the already established manufacturing process for the commercial heating film by SH Korea Co. required the injection of the smallest possible amount of sample J, because a considerable amount of sample J may cause poor adhesion between the paste layer and the PET substrate. The PET film coated with the 2 wt% sample J-incorporated carbon paste seemed to satisfy the adhesion problem, as well as provide good SE values, as shown in Figure 6.

For the manufacturing process of the commercial heating film, we used a coated PET film with 5 wt% sample J-incorporated carbon paste. In this case, we used a typical laminating process using the gravure method of SH Korea Co. The typical thickness of the coated layer using carbon paste was approximately 50 μm . Basically, a single des-HF was composed of two electromagnetic wave shielding layers located at the front and back sides among eight different functional individual thin layers. Therefore, we estimated a total thickness of 100 μm for the coated layers using 5 wt% sample J-incorporated carbon paste.

Figure 7 shows the total SE values for the conventional heating film using native commercial carbon paste, des-HF manufactured by 5 wt% sample E-incorporated carbon paste, and des-HF manufactured by 5 wt% sample J-incorporated carbon paste. As discussed in the results depicted in Figure 6, the total SE values of the native conventional heating film using commercial carbon paste were enhanced by the incorporation of 5 wt% sample E, and further enhanced by the incorporation of 5 wt% sample J. The cause for the improvement of the SE values seems to be largely attributable to the fact that numerous small CNFs intersected with one another and/or the intrinsic characteristics of CMCs; however, the electrical conductivity of the coated PET film using the commercial carbon paste was decreased by the incorporation of controllable CMCs, or hybrids of CNFs–CMCs in the commercial carbon paste (see Table 1).

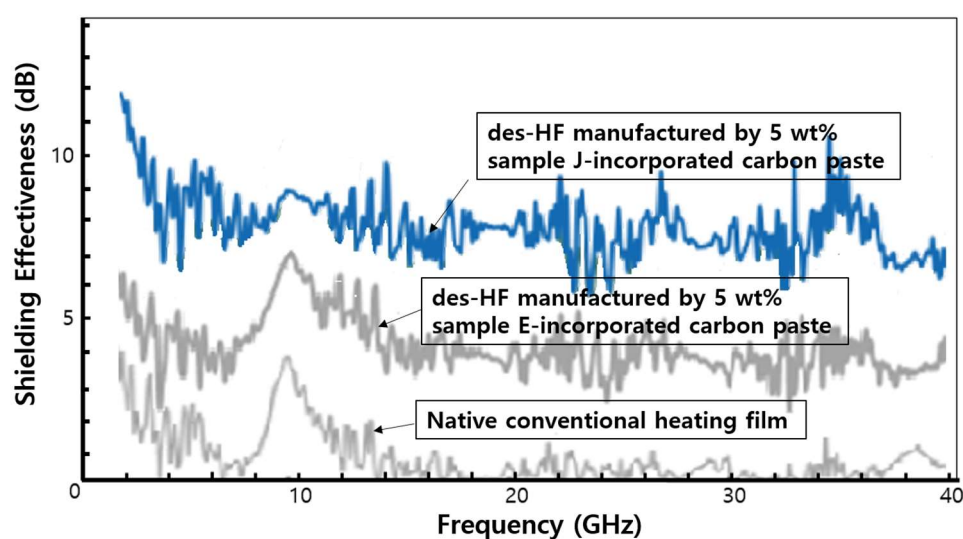


Figure 7. The total SE values for the conventional heating film using native commercial carbon paste, the des-HF manufactured by 5 wt% sample-E incorporated carbon paste, and the des-HF manufactured by 5 wt% sample-J incorporated carbon paste.

Figure 8 shows the total SE values, the SE values for the absorption loss, and the SE values for the reflection loss of the des-HF manufactured by 5 wt% sample J-incorporated carbon paste across the operating frequencies in the 1.5–40 GHz range. Above the 4.0 GHz frequency range, the absorption SE values of the des-HF manufactured by 5 wt% sample J-incorporated carbon paste increased and approached the values of the total SE values, as shown in Figure 8. This confirms that the higher total SE values of the hybrids of CNFs–CMCs in this work are mainly attributable to the enhanced absorption loss across the operating frequencies in the 4.0–40 GHz range. Therefore, the enhanced total SE values obtained using the hybrids of CNFs–CMCs were mainly ascribed to the enhanced absorption shielding loss, contributed by the intrinsic characteristics of CMCs and the aspect of numerous small-sized CNFs intersecting with one another in sample J.

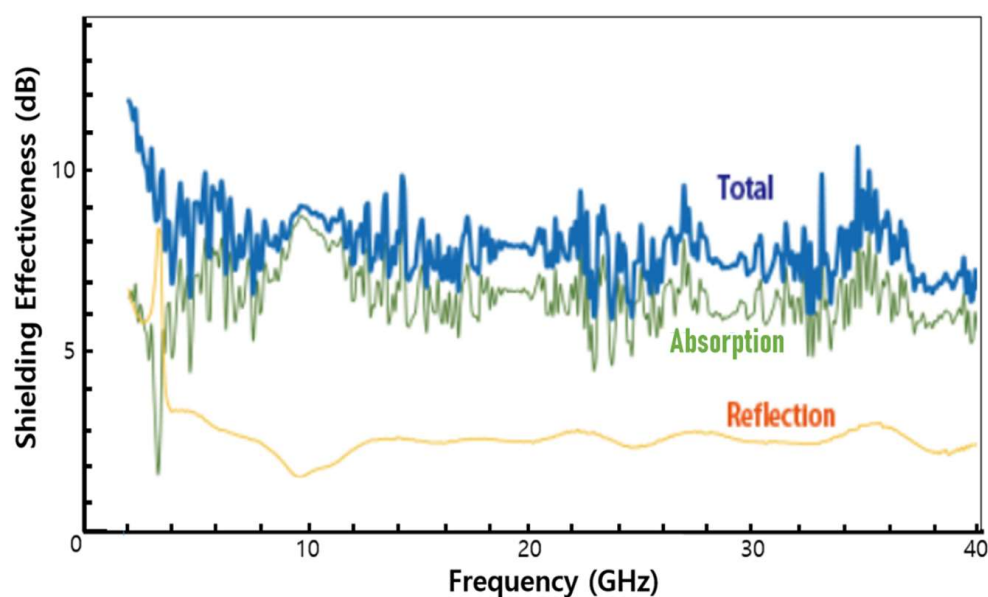


Figure 8. Total SE values, the SE values for the reflection loss, and the SE values for the absorption loss of the des-HF manufactured by 5 wt% sample J-incorporated carbon paste.

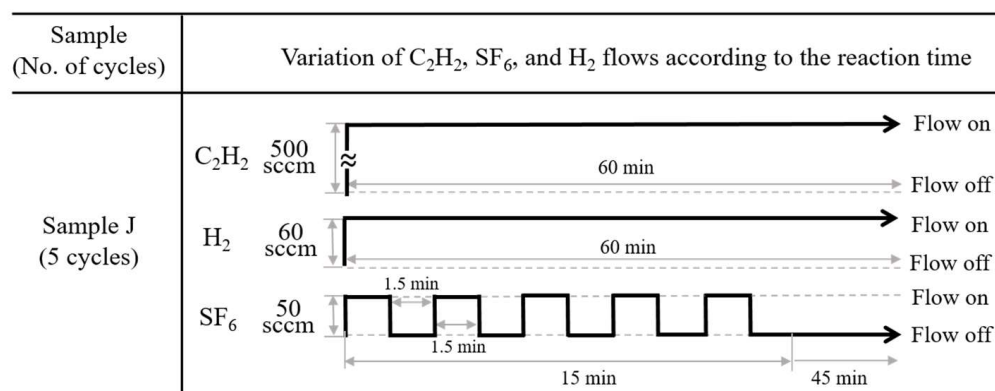
3. Materials and Methods

As a catalyst for the formation of CMCs, approximately 0.1 g of bunch-type Ni powder (99.7%), with particle diameters ranging from 1 μm to 10 μm , was spread onto a 2 mm-thick, boat-like stainless steel (SUS304) substrate. A thermal chemical vapor deposition (CVD) system was employed for the formation of CMCs, using C_2H_2 as the source gas and SF_6 as the additive gas. The deposition reaction conditions for the formation of the various CMCs-related samples are listed in Table 3. Ten samples (samples A–J) with different combinations of gas flow rate, gas flow injection time, and gas type were prepared.

Regarding the application of SF_6 gas in sample J, the cyclic process was conducted by simply switching the SF_6 flow on and off continuously. The gas flow sequence mirrored the iterative order of the reaction processes: $\text{C}_2\text{H}_2 + \text{H}_2 + \text{SF}_6$ flow (C_2H_2 flow-on, H_2 flow-on, and SF_6 flow-on) followed by $\text{C}_2\text{H}_2 + \text{H}_2$ flow (C_2H_2 flow-on, H_2 flow-on, and SF_6 flow-off), as shown in Figure 9. The cycle period was defined as the sum of the time the source gases were composed of $\text{C}_2\text{H}_2 + \text{H}_2 + \text{SF}_6$ flow, and the time the source gases consisted solely of $\text{C}_2\text{H}_2 + \text{H}_2$ flow. For sample J, the on and off times for the SF_6 flow injection were set at 1.5 min, resulting in a total duration of 3.0 min for one cycle. Because the total cyclic on/off modulation of the SF_6 flow was 15 min, five cycles were performed during the reaction.

Table 3. Experimental conditions for Samples A–J.

Sample	C ₂ H ₂ Flow Rate (sccm)	H ₂ Flow Rate (sccm)	SF ₆ Flow Rate (sccm)	SF ₆ Flow Injection Time (min)	No. of SF ₆ Flow On/Off Cycles	Total Reaction Time (min)	Total Gas Pressure (Torr)	Substrate Temp. (°C)	Remarks
A	500	-	20	5	-	60	100	750	Without cyclic process
B	500	-	20	15	-	60	100	750	Without cyclic process
C	500	-	20	30	-	60	100	750	Without cyclic process
D	500	-	50	5	-	60	100	750	Without cyclic process
E	500	-	50	15	-	60	100	750	Without cyclic process
F	500	-	50	30	-	60	100	750	Without cyclic process
G	500	-	100	5	-	60	100	750	Without cyclic process
H	500	-	100	15	-	60	100	750	Without cyclic process
I	500	-	100	30	-	60	100	750	Without cyclic process
J	500	60	50	15	5	60	100	750	With cyclic process of SF ₆ flow

**Figure 9.** Cyclic injection processes of C₂H₂, H₂, and SF₆ flows for sample J.

The morphologies of the CMCs samples were investigated in detail by field emission scanning electron microscopy (FESEM; S-4200 Hitachi, Tokyo, Japan). The thickness of the sample was measured using a micrometer (406-250-30 Mitutoyo, Nakagawa, Japan) and corrected using cross-sectional FESEM images. Resistivity values were obtained by using a four-point probe (labsysstc-400 Nextron, Busan, Republic of Korea) connected to a source meter (2400 Source Meter Keithley, Cleveland, OH, USA) and by performing calculations using Ohm's law with a correction factor, according to the method proposed by Smits [32]. The four-point probe system consisted of four, straight-lined probes with an equal inter-probe spacing of 3.0 mm. A constant current (I) was supplied through the two outer probes, and the output voltage (V) was measured using the two inner probes [31]. Correction factors (C and F) were obtained from Smits et al. [32]. Surface and volume resistivities were calculated using the following equations [32,33]:

$$\text{Surface resistivity : } \rho_s = \frac{V}{I} C \left(\frac{a}{d}, \frac{d}{s} \right), \text{ volume resistivity : } \rho_v = \rho_s w F \left(\frac{w}{s} \right)$$

where a , d , w , and s denote the length, width, and thickness of the sample and the inter-probe spacing, respectively.

The final product of the heating films, namely dual electromagnetic shielding premium heating films (des-HFs), were prepared by a typical laminating process with the gravure method of SH Korea Co. (see Figure 10) using the blends of CMCs-related samples and

commercially supplied carbon paste. 2-butoxyethyl acetate was used as the diluting solution during the gravure coating process with these blends.

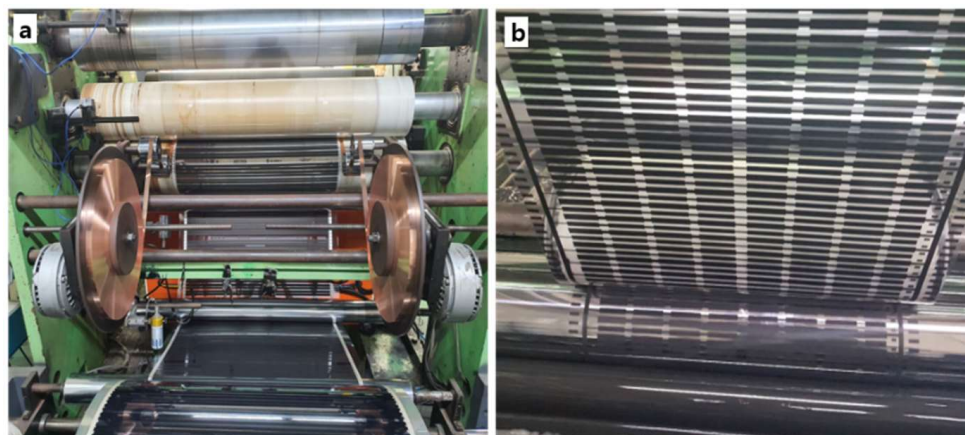


Figure 10. The production of heating film: (a) the coating equipment used to perform the gravure method and (b) the actual gravure coating process of carbon paste on the base film.

A single des-HF film was composed of eight different functional individual thin films, as shown in Figure 11.

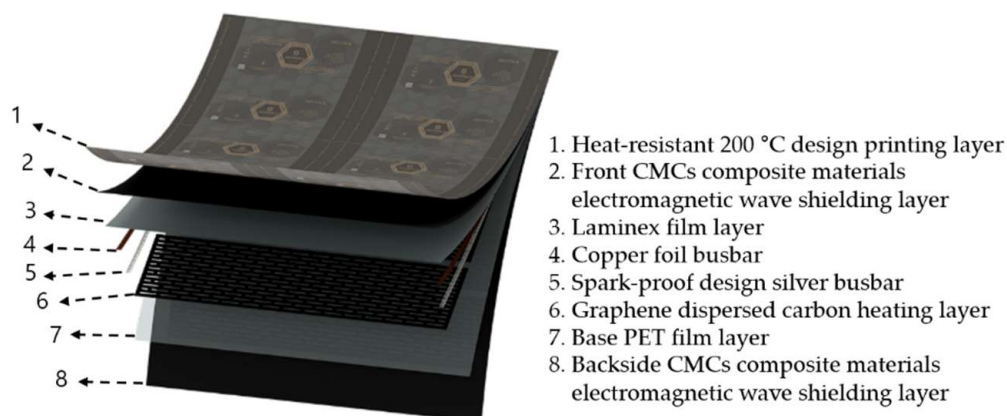


Figure 11. Structure of dual electromagnetic shielding premium heating film.

The SE values of the des-HFs were measured using a waveguide method with a vector network analyzer (VNA; 37369C Anritsu, Kanagawa, Japan), as shown in Figure 12. The results were compared with those of a heating film made using commercially available carbon paste (CKC-300 AF Electrochem, Incheon, Republic of Korea). The setup for the VNA system consisted of a sample holder with its exterior connected to the system. A coaxial sample holder and a coaxial transmission test specimen were set up according to the waveguide method. The scattering parameters (S_{11} and S_{21}) were measured in the frequency range of 1.5–40 GHz using the VNA [34–38]. The power coefficients, namely reflectivity (R), absorptivity (A), and transmissivity (T), were calculated using the following equations: $R = P_R/P_I = |S_{11}|^2$ and $T = P_T/P_I = |S_{21}|^2$, where P_I , P_R , P_A , and P_T are the incident, reflected, absorbed, and transmitted powers of an electromagnetic wave, respectively [38]. The power coefficient relationships were expressed as $R + A + T = 1$. The SE of the electromagnetic waves was calculated from the scattering parameters using the following equation:

$$SE_{\text{Tot}} = -10 \log T, \quad (1)$$

$$SE_R = -10 \log (1 - R), \quad (2)$$

$$SE_A = -10 \log\{T/(1 - R)\}, \quad (3)$$

where, SE_{Tot} , SE_R , and SE_A denote the total, reflection, and absorption SE values, respectively [37,38].

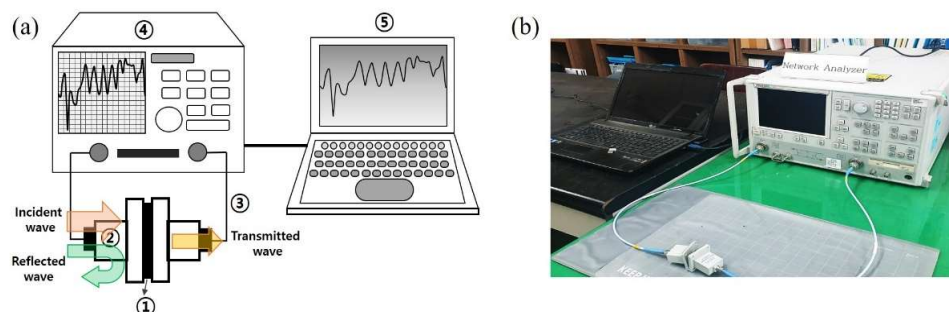


Figure 12. (a) Schematic of the vector network analyzer (VNA): ① sample, ② waveguide test holders, ③ coaxial cables, ④ VNA, and ⑤ computer and (b) optical photograph of the experimental setup for the EMI shielding measurements.

4. Conclusions

Controllable CMCs, especially the controlled-diameter size of CMCs, could be achieved by manipulating the injection gas parameters under $C_2H_2 + SF_6$ gas flow in a thermal chemical vapor deposition system. The diameters of the CMCs were independent of the SF_6 flow rate, but strongly dependent on the SF_6 flow injection time. The cyclic process of SF_6 flow with the injection of H_2 flow could produce the formation of CNFs–CMCs hybrid. The formation of the hybrids of CNFs–CMCs by the cyclic process of SF_6 flow with the injection of H_2 flow was explained by the generation of a large number of tiny Ni catalysts to overcome the deficiency of tiny Ni catalysts on the surfaces of the CMCs. This was attributed to the facile diffusion of Ni catalysts into the interior of the CMCs during the reaction. Systematic diagrams were deployed to assist the different formation of the controllable CMCs and hybrids of CNFs–CMCs, according to the different gas injection aspects.

For one batch reaction, approximately 20 g of the hybrids of CNFs–CMCs with numerous small-sized CNFs around the CMCs was obtained by about 0.6 g Ni catalyst onto a 2mm-thick, boat-like stainless steel (SUS304) substrate.

Compared with the total SE values of the PET film coated with 30 wt% controllable CMCs-incorporated carbon paste, the values of the PET film coated with 30 wt% hybrids of CNFs–CMCs incorporated carbon paste were more than two-fold higher in dB scale across the entire operating frequency range. This dramatic increase in the total SE values was partly ascribed to the enhanced electrical conductivity, due to the hybrid formation between the numerous small CNFs and the CMCs. Furthermore, the intrinsic characteristics of CMCs and the behavior of numerous small-sized CNFs intersecting with one another in the CNFs–CMCs hybrids can enhance the magnetic field and absorb incoming EM waves. Consequently, they can improve the absorption loss of electromagnetic waves. Therefore, the SE values of the PET film coated with the hybrids of CNF-CMCs incorporated carbon paste were much higher than those with 30 wt% controllable CMCs incorporated carbon paste across the entire operating frequency range.

Although the electrical conductivity of the coated PET film using the commercial carbon paste was decreased by the incorporation of the hybrids of CNFs–CMCs in the commercial carbon paste, the total SE values of the conventional heating film using the commercial carbon paste were significantly enhanced by the incorporation of 5 wt% hybrids of CNFs–CMCs. The cause for this dramatic enhancement of the SE could be attributable to the fact that numerous small-sized CNFs intersect with one another and the intrinsic characteristics of CMCs.

Author Contributions: Conceptualization, S.-H.K. and G.-H.K.; methodology, G.-H.K. and J.-H.K.; validation, G.-H.K. and S.-H.K.; formal analysis, G.-H.K., J.-H.K. and J.L.; investigation, G.-H.K., J.L. and S.-H.K.; resources, S.-H.K. and Y.T.K.; data curation, G.-H.K., M.H.Y. and S.-H.K.; writing—original draft preparation, S.-H.K. and G.-H.K.; writing—review and editing, G.-H.K. and S.-H.K.; visualization, G.-H.K. and J.-H.K.; supervision, S.-H.K.; project administration, S.-H.K. and M.H.Y.; funding acquisition, S.-H.K. and Y.T.K. All authors contributed to the general discussion. All authors have read and agreed to the published version of the manuscript.

Funding: This research was supported by the Basic Science Research Program through the National Research Foundation of Korea (NRF), funded by the Ministry of Education (NRF-2021R1I1A3047330). This work was also supported by the Nano-Convergence Foundation (www.nanotech2020.org (accessed on 9 October 2021)) funded by the Ministry of Science and ICT (MSIT, Korea) and the Ministry of Trade, Industry and Energy (MOTIE, Korea). Project Name: Development of Hot Film Module based on Nanocarbon Hybrid Colloid Composite Solution to Shield Wide Range Electromagnetic Wave Radiation/Project Number: R202101800. This work was also supported by the BB21+ Project in 2018.

Institutional Review Board Statement: Not applicable.

Informed Consent Statement: Not applicable.

Data Availability Statement: All data used and/or analyzed during the current study are shown within the study. If further data are required, they can be made available by the corresponding author upon reasonable request.

Conflicts of Interest: The authors declare no conflict of interest.

References

- Schulz, R.B.; Plantz, V.C.; Brush, D.R. Shielding theory and practice. *Inst. Electr. Electron. Eng.* **1988**, *30*, 187–201. [[CrossRef](#)]
- Chung, D.L. Materials for Electromagnetic Interference Shielding. *J. Mater. Eng. Perform.* **2000**, *9*, 350–354. [[CrossRef](#)]
- Al-Saleh, M.H.; Sundararaj, U. Electromagnetic Interference Shielding Mechanisms of CNT/polymer Composites. *Carbon* **2009**, *47*, 1738–1746. [[CrossRef](#)]
- Simon, R.M. EMI Shielding Through Conductive Plastics. *Polym.-Plast. Technol. Eng.* **1981**, *17*, 1–10. [[CrossRef](#)]
- Chung, D.L. Electromagnetic Interference Shielding Effectiveness of Carbon Materials. *Carbon* **2001**, *39*, 279–285. [[CrossRef](#)]
- Yang, Y.; Gupta, M.C.; Dudley, K.L.; Lawrence, R.W. Novel carbon, nanotube polystyrene foam composites for electromagnetic interference shielding. *Nano Lett.* **2005**, *5*, 2131–2134. [[CrossRef](#)]
- Ameli, A.; Nofar, M.; Wang, S.; Park, C.B. Lightweight polypropylene/stainless steel fiber composite foams with low percolation for efficient electromagnetic interference shielding. *ACS Appl. Mater. Interfaces* **2014**, *6*, 11091–11100. [[CrossRef](#)]
- Ling, J.; Zhai, W.; Feng, W.; Shen, B.; Zhang, J.; Zheng, W. Facile preparation of lightweight microcellular polyetherimide/graphene composite foams for electromagnetic interference shielding. *ACS Appl. Mater. Interfaces* **2013**, *5*, 2677–2684. [[CrossRef](#)]
- Zeng, Z.; Jin, H.; Chen, M.; Li, W.; Zhou, L.; Xue, X. Microstructure design of lightweight, flexible, and high electromagnetic shielding porous multi walled carbon nanotube/polymer composites. *Small* **2017**, *13*, 1701388. [[CrossRef](#)]
- Arjmand, M.; Sundararaj, U. Electromagnetic interference shielding of nitrogen-doped and undoped carbon nanotube/polyvinylidene fluoride Nanocomposites: A Comparative Study. *Compos. Sci. Technol.* **2015**, *118*, 257–263. [[CrossRef](#)]
- Liang, J.; Wang, Y.; Huang, Y.; Ma, Y.; Liu, Z. Electromagnetic interference shielding of graphene/epoxy composites. *Carbon* **2009**, *47*, 922–925. [[CrossRef](#)]
- Rahman, M.J.; Mieno, T. Conductive Cotton Textile from Safely Functionalized Carbon Nanotubes. *J. Nanomater.* **2015**, *2015*, 978484. [[CrossRef](#)]
- Tarek, R.; Cemal, B. Joule heating in single-walled carbon nanotubes. *J. Appl. Phys.* **2009**, *106*, 063705.
- Ren, J.; Wang, C.; Zhang, X.; Carey, T.; Chen, K.; Yin, Y.; Torrisi, F. Environmentally friendly conductive cotton fabric as flexible strain sensor based on hot press reduced graphene oxide. *Carbon* **2017**, *111*, 622–630. [[CrossRef](#)]
- Ahmed, A.; Jalil, M.A.; Hossain, M.M.; Moniruzzaman, M.; Adak, B.; Islam, M.T.; Parvez, M.S. PEDOT: PSS and graphene-clad smart textile-based wearable electronic joule heater with high thermal stability. *J. Mater. Chem. C* **2020**, *8*, 16204–16215. [[CrossRef](#)]
- Koçanalı, A.; Apaydın Varol, E. An Experimental study on the electrical and thermal performance of reduced graphene oxide coated cotton fabric. *Int. J. Energy Res.* **2021**, *45*, 12915–12927. [[CrossRef](#)]
- Pereira, P.; Ferreira, D.P.; Araújo, J.C.; Ferreira, A.; Figueiro, R. The potential of graphene nanoplatelets in the development of smart and multifunctional eco-composites. *Polymers* **2020**, *12*, 2189. [[CrossRef](#)]
- Moreira, I.P.; Sanivada, U.K.; Bessa, J.; Cunha, F.; Figueiro, R. A review of multiple scale fibrous and composite systems for heating applications. *Molecules* **2021**, *26*, 3686. [[CrossRef](#)]
- Chungjae, L.E.E. A Film Heater Having Offsetted Electron of Wave. Korean Patent KR102075870, 2020.

20. Kim, J.S.; Kim, D.A.; Park, S.T.; Kang, M.S. The Product Method of Heating Film for Electro Magnetic Shielding. Korean Patent KR101620503, 2016.
21. Kang, S.; Choi, H.; Lee, S.B.; Park, S.C.; Park, J.B.; Lee, S.; Kim, Y.; Hong, B.H. Efficient heat generation in large-area graphene films by electromagnetic wave absorption. *2D Mater.* **2017**, *4*, 025037. [[CrossRef](#)]
22. Lin, C.-L.; Li, J.-W.; Chen, Y.-F.; Chen, J.-X.; Cheng, C.-C.; Chiu, C.-W. Graphene Nanoplatelet/Multiwalled Carbon Nanotube/Polypyrrole Hybrid Fillers in Polyurethane Nanohybrids with 3D Conductive Networks for EMI Shielding. *ACS Omega* **2022**, *7*, 45697–45707. [[CrossRef](#)]
23. Wang, M.; Tang, X.H.; Cai, J.-H.; Wu, H.; Shen, J.-B.; Guo, S.-Y. Fabrication, mechanisms and perspectives of conductive polymer composites with multiple interfaces for electromagnetic interference shielding: A review. *Carbon* **2021**, *177*, 377–402. [[CrossRef](#)]
24. Davis, W.R.; Slawson, R.J.; Rigby, G.R. An Unusual form of carbon. *Nature* **1953**, *171*, 756. [[CrossRef](#)]
25. Motojima, S.; Hoshiya, S.; Hishikawa, Y. Electromagnetic wave absorption properties of carbon microcoils/PMMA composite beads in W bands. *Carbon* **2003**, *41*, 2658–2660. [[CrossRef](#)]
26. Motojima, S.; Noda, Y.; Hoshiya, S.; Hishikawa, Y. Electromagnetic wave absorption property of carbon microcoils in 12–110 GHz region. *J. Appl. Phys.* **2003**, *94*, 2325. [[CrossRef](#)]
27. Zhao, D.L.; Shen, Z.M. Preparation and microwave absorption properties of carbon nanocoils. *Mater. Lett.* **2008**, *62*, 3704–3706. [[CrossRef](#)]
28. Kang, G.-H.; Kim, S.-H. Electromagnetic wave shielding effectiveness based on carbon microcoil-polyurethane composites. *J. Nanomater.* **2014**, *2014*, 727024. [[CrossRef](#)]
29. Kim, H.-J.; Kim, S.-H.; Park, S. Effects of the carbon fiber-carbon microcoil hybrid formation on the effectiveness of electromagnetic wave shielding on carbon fibers-based fabrics. *Materials* **2018**, *11*, 2344. [[CrossRef](#)] [[PubMed](#)]
30. Kang, G.-H.; Kim, S.-H.; Park, S. Enhancement of shielding effectiveness for electromagnetic wave radiation using carbon nanocoil-carbon microcoil hybrid materials. *Appl. Surf. Sci.* **2019**, *447*, 264–270. [[CrossRef](#)]
31. Pothupitiya, G.S.J.; Yang, K.; Braveenth, R.; Raagulan, K.; Kim, H.S.; Lee, Y.S.; Yang, C.-M.; Moon, J.J.; Chai, K.Y. MWCNT coated free-standing carbon fiber fabric for enhanced performance in EMI shielding with a higher absolute EMI SE. *Materials* **2017**, *10*, 1350. [[CrossRef](#)]
32. Smits, F. Measurement of Sheet Resistivities with the Four-Point Probe. *Bell Syst. Tech. J.* **1958**, *37*, 711–718. [[CrossRef](#)]
33. Shuying, Y.; Karen, L.; Azalia, L.; Heinrich, D.F.; Robert, J. Electromagnetic Interference Shielding Effectiveness of Carbon Nanofiber/LCP Composites. *Compos. Part A Appl. Sci. Manuf.* **2005**, *36*, 691–697.
34. Pütz, J.; Heusing, S.; Aegerter, M.A. Characterization of Electrical Properties. In *Handbook of Sol-Gel Science and Technology*; Kluwer Academic Publishers: Amsterdam, The Netherlands, 2016.
35. Song, W.L.; Cao, M.S.; Lu, M.M.; Bi, S.; Wang, C.Y.; Liu, J.; Yuan, J.; Fan, L.Z. Flexible Graphene/Polymer Composite Films in Sandwich Structures for Effective Electromagnetic Interference Shielding. *Carbon* **2014**, *66*, 67–76. [[CrossRef](#)]
36. Song, W.L.; Wang, J.; Fan, L.Z.; Li, Y.; Wang, C.Y.; Cao, M.S. Interfacial Engineering of Carbon Nanofiber@Graphene@Carbon Nanofiber Heterojunctions in Flexible Lightweight Electromagnetic Shielding Networks. *ACS Appl. Mater. Interface* **2014**, *6*, 10516–10523. [[CrossRef](#)] [[PubMed](#)]
37. Cao, M.S.; Song, W.L.; Hou, Z.L.; Wen, B.; Yuan, J. The Effects of Temperature and Frequency on the Dielectric Properties, Electromagnetic Interference Shielding and Microwave-Absorption of Short Carbon Fiber/Silica Composites. *Carbon* **2010**, *48*, 788–796. [[CrossRef](#)]
38. Huang, H.D.; Liu, C.Y.; Zhou, D.; Jiang, X.; Zhong, G.J. Cellulose Composite Aerogel for Highly Efficient Electromagnetic Interference Shielding. *J. Mater. Chem. A* **2015**, *3*, 4983–4991. [[CrossRef](#)]
39. Kang, G.-H.; Kim, S.-H.; Park, S. Controllable synthesis of carbon-nanocoil—carbon-microcoil hybrid materials. *Mater. Des.* **2016**, *116*, 42–50. [[CrossRef](#)]
40. Kim, H.-J.; Kang, G.-H.; Kim, S.-H.; Park, S. Enhancement in Electromagnetic Wave Shielding Effectiveness through the Formation of Carbon Nanofiber Hybrids on Carbon-Based Nonwoven Fabrics. *Nanomaterials* **2021**, *11*, 2910. [[CrossRef](#)]
41. Zhu, S.; Su, C.H.; Lehoczy, S.L.; Muntele, I.; Ila, D. Carbon nanotube growth on carbon fibers, *Diam. Relat. Mater.* **2003**, *12*, 1825–1828. [[CrossRef](#)]
42. Zhao, Z.G.; Ci, L.J.; Cheng, H.M.; Bai, J.B. The growth of multi-walled carbon nanotubes with different morphologies on carbon fibers. *Carbon* **2005**, *43*, 651–673. [[CrossRef](#)]
43. Shaikjee, A.; Coville, N.J. The synthesis, properties and uses of carbon materials with helical morphology. *J. Adv. Res.* **2012**, *3*, 195–223. [[CrossRef](#)]
44. Nishino, T.; Naito, H.; Nakamura, K.; Nakamae, K. X-ray diffraction studies on the stress transfer of transversely loaded carbon fibre reinforced composite. *Compos. Part A* **2000**, *31*, 1225–1230. [[CrossRef](#)]
45. Qiu, T.; Yang, J.-G.; Bai, X.-J.; Wang, Y.-L. The preparation of synthetic graphite materials with hierarchical pores from lignite by one-step impregnation and their characterization as dye absorbents. *RSC Adv.* **2019**, *9*, 12737. [[CrossRef](#)] [[PubMed](#)]
46. Kang, G.-H.; Bae, M.-K.; Kim, S.-H. Formation of noble-shaped carbon nanostructures. *J. Incl. Phenom. Macrocycl. Chem.* **2015**, *82*, 179–186. [[CrossRef](#)]
47. Anisha, C.; Saroj, K.; Rajeev, K. Lightweight and Easily Foldable MCMB-MWCNTs Composite Paper with Exceptional Electromagnetic Interference Shielding. *ACS Appl. Mater. Interfaces* **2016**, *8*, 16.

48. Al-Saleh, M.H.; Saadeh, W.H.; Sundararaj, U. EMI shielding effectiveness of carbon based nanostructured polymeric materials: A comparative study. *Carbon* **2013**, *60*, 146–156. [[CrossRef](#)]
49. Lv, X.; Yang, S.; Jin, J. Preparation and electromagnetic properties of carbon nanofiber/epoxy composites. *J. Macromol. Sci. B* **2010**, *49*, 355–365. [[CrossRef](#)]
50. Nidhi, A.; Kuntal, C. Highly efficient electromagnetic interference shielding using graphite nanoplatelet/poly(3,4-ethylenedioxythiophene)-poly(styrenesulfonate) composites with enhanced thermal conductivity. *RSC Adv.* **2015**, *5*, 43765–43771.
51. Das, N.C.; Khastgir, D.; Chaki, T.K.; Chakraborty, A. Electromagnetic interference shielding effectiveness of carbon black and carbon fibre filled EVA and NR based composites. *Compos. Part A* **2000**, *31*, 1069–1081. [[CrossRef](#)]
52. Fan, Z.; Wang, D.; Yuan, Y.; Wang, Y.; Cheng, Z.; Liu, Y.; Xie, Z. A lightweight and conductive MXene/graphene hybrid foam for superior electromagnetic interference shielding. *Chem. Eng. J.* **2020**, *381*, 122696. [[CrossRef](#)]
53. Lee, S.-H.; Kang, D.; Oh, I.-K. Multilayered graphene-carbon nanotube-iron oxide three-dimensional heterostructure for flexible electromagnetic interference shielding film. *Carbon* **2017**, *111*, 248–257. [[CrossRef](#)]
54. Wang, Z.; Mao, B.; Wang, Q.; Yu, J.; Dai, J.; Song, R.; Pu, Z.; He, D. Ultrahigh Conductive Copper/Large Flake Size Graphene Heterostructure Thin-Film with Remarkable Electromagnetic Interference Shielding Effectiveness. *Small* **2018**, *14*, e1704332. [[CrossRef](#)] [[PubMed](#)]
55. Li, N.; Huang, Y.; Du, F.; He, X.; Lin, X.; Gao, H.; Ma, Y.; Li, F.; Chen, Y.; Eklund, P.C. Electromagnetic Interference (EMI) Shielding of Single-Walled Carbon Nanotube Epoxy Composites. *Nano Lett.* **2006**, *6*, 1141–1145. [[CrossRef](#)] [[PubMed](#)]

Disclaimer/Publisher's Note: The statements, opinions and data contained in all publications are solely those of the individual author(s) and contributor(s) and not of MDPI and/or the editor(s). MDPI and/or the editor(s) disclaim responsibility for any injury to people or property resulting from any ideas, methods, instructions or products referred to in the content.